Polymer-lipid hybrid membranes as a model platform to drive membrane-cytochrome c interaction and peroxidase-like activity

Stefano Di Leone[a,b], *Saziye Yorulmaz Avsar*[a], *Andrea Belluati*[a], *Riccardo Wehr*[a], *Cornelia G. Palivan*[a], *Wolfgang Meier*[a]

[a]Chemistry Department, University of Basel, BPR 1096, Mattenstrasse 24a, 4058 Basel, Switzerland.

[b]School of Life Sciences, Institute for Chemistry and Bioanalytics, University of Applied Sciences Northwestern Switzerland (FHNW), Grundenstrasse 40, 4132 Muttenz

ABSTRACT

Controllable attachment of proteins to material surfaces is very attractive for many applications including biosensors, bioengineered scaffolds or drug screenings. Especially, redox proteins have received considerable attention as a model system not only to understand mechanism of electron transfer in biological systems but also development of novel biosensors. However, current research attempts suffer from denaturation of the protein after its attachment to solid substrates. Here, we present how lipid, polymer and hybrid membranes based on mixtures of lipids and copolymers on solid support provide more favourable environment to drive selective and functional attachment of a model redox protein, cytochrome c (cyt c). Polymer membranes provided chemical versatility to support

covalent attachment of cyt c, whereas lipid membranes provided flexibility and biocompatibility to support insertion of cyt c through its hydrophobic part. Hybrid membranes combined the most promising characteristics of both lipids and polymers and allow attachment of cyt c with both covalent attachment and insertion driven by hydrophobic interactions. We then investigated the effect of different attachment strategies on the accessibility and peroxidase like activity of cyt c, in presence of the different membranes. The real-time combination of cyt c with the planar membranes was investigated by quartz crystal microbalance with dissipation (QCM-D). It was possible to selectively drive the insertion of the cyt c into a specific lipid domain of hybrid membranes. In addition, protein accessibility and its functionality were dependent on the specificity of the combination strategy: covalent conjugation of cyt c to polymer and hybrid membranes promoted higher accessibility and supported higher peroxidase-like activity. Taking together, the combination of biomolecules with planar membranes can be modulated such to improve the accessibility of the biomolecules and their resulting functionality for development of efficient "active surfaces".

Introduction

Cell membranes consist of phospholipids, glycolipids and a large variety of proteins, responsible for active or passive transport and signalling[1]. One strategy to understand how biological membranes are associated with proteins, to support biological processes, is to utilize model membrane platforms. To date, naturally occurring or synthetic phospholipids and amphiphilic block copolymers have been used to create model membrane platforms[2-4] in combination with a variety of different biomolecules including proteins, peptides and receptors. So far, synthetic membranes have been characterized in a three-dimensional assembly (e.g. liposomes, polymersomes, giant vesicles), which has been not always straightforward, due to the challenges associated with characterization of vesicular model systems. Therefore, supported membrane formation by single component (e.g. lipids or polymers) emerged[5-9].

Deposition of planar membrane on solid support present as advantages compared vesicular membranes[10]; (i) a higher amenability for characterization by surface sensitive analytical tools (e.g. atomic force microscopy(AFM), quartz crystal microbalance with dissipation (QCM-D), and surface plasmon resonance (SPR)) and thus the investigation of protein-membrane interaction kinetics in real-time, *in situ* and label-free format[11] and (ii) the possibility to pattern the surface to monitor membrane phase separation[12] and selective molecular binding[13].

In addition to single component membrane platforms, phospholipids and block copolymers have been mixed to form hybrid membranes[5-6, 12]. Within hybrid membranes, amphiphilic block copolymers provide improved mechanical and structural stability while phospholipids can provide a better environment for integration of biomolecules[12, 14-16]. Depending on how lipid and polymer chains are distributed within hybrid membranes, an enhanced control of membrane functionalization with different biomolecules (e.g. proteins) can be achieved[17-20]. In fact, hybrid membranes can undergo phase domain separation when the fluid phase polymer and gel phase lipids are used to prepare them and this significantly affects proteins-membrane interaction[21]. Additionally, phase domains in hybrid membranes have been created by changing the molar ratio of each component and molecular parameters of lipids and block copolymers, such as phase transition temperature and composition [12, 22-24]. The control over the membrane-protein combination is essential for the development of "active surfaces" with desired properties. Although most of the hybrid membrane studies have been focused on the mixing of lipids and block copolymers in vesicles, only a few studies have explored the properties of the hybrid membranes on solid supports and their combinations with proteins (e.g. P-glycoprotein) and peptides (e.g. gramicidin A and valynomicyn)[21, 25-27].

Planar membranes on solid support are obtained by either substrate mediated vesicle fusion [28-29] or Langmuir Blodgett transfer method[19, 28], while their characterisation is achieved by a combination of surface methods including QCM-D, AFM and ellipsometry[12]. Due to the capability of lipids and

copolymers to re-arrange the membrane architecture and generate domains, hybrid membranes represent ideal candidates for understanding protein-membrane interactions[30]. These domains facilitate the interaction with proteins, in a way similar to the so-called "lipid-rafts" found in cell membranes[15, 30]. For example, when the DPPC lipids (phase transition temperature of 41°C) were mixed with the PMOXA-*b*-PDMS block copolymer at room temperature, proteins selectively inserted only into the polymer domains because the lipid domains were in gel-phase and they did not support insertion of the proteins [12]. The advantage of combining proteins with synthetic planar membranes relies in preserving protein activity, which can be prohibited when a protein is directly attached to a bare substrate surface, such as gold, silica or glass[31-35]. Attachment of proteins with different solid substrates are mainly based on noncovalent interactions, such as ionic or hydrogen bonds and often induces a protein denaturation. For example, it is well known that functional properties of cytochrome c (cyt c) was hampered because it adsorbed strongly on electrodes (e.g. Pt, Hg, Au and Ag) since this adsorption caused large conformational changes and denaturation[36-38]. Moreover, direct electron transfer between cytochrome c and unmodified electrode surface is slow due to undesired contact between the prosthetic group and the electrode[39]. So far, in order to provide a better environment for cyt c to function, different electrodes which are mainly based on nanomaterials (e.g. carbon nanotubes, graphene and nanoparticles) have been used[40-45]. Nevertheless, these attempts might not be sufficient to preserve the whole cyt c activity. By forming planar membranes on solid support as a mean of electrode surface modification, (i) a natural biocompatible means of cyt c-substrate interactions, and (ii) effective, highly dynamic platform to host biomolecules can be achieved[46-47]. Such system improves the protein-membrane-substrate communication for development of highly sensitive and efficient biosensors.

Here we combine different solid-supported membranes based on lipids, copolymers and mixtures of lipids and copolymers with cytochrome c, a model protein in order to understand which molecular factors are playing a crucial role in its accessibility and functionality. We attached the cyt c by two

different approaches, one based on insertion mediated by hydrophobic interactions and a second one by covalent conjugation of the cyt c with specific functional groups of the copolymer. More specifically, cyt c is a critical signalling molecule, leading to activation of enzymes in the intrinsic pathway of apoptosis upon permeabilization of upper layer of mitochondrial membrane[48-51]. It has a relatively small size of 12 kDa with globular shape and it is known that its binding to the membranes can be driven by either ionic interactions or small hydrophobic domains which drives the spontaneous insertion[51-52]. Moreover, the presence of amine groups of two specific external lysines (Lys72 and Lys73) supports cyt c to be covalently conjugated to the carboxylic groups of the copolymer in the membranes. To date, the combination of cyt c with the biologic membranes mainly takes places through electrostatic interaction with negatively charged surfaces, due to two residual lysines, partial insertion via hydrophobic interaction or complete incorporation into the membrane[52-53]. Both electrostatic and hydrophobic interactions plaid a role on cyt c combination with membranes based on anionic lipids[54-56]. The contribution of the hydrophobic interaction on cyt c insertion has been studied by using zwitterionic lipid membranes and the results indicated that cyt c induced the disruption of the membrane[57]. To preserve membrane integrity, another approach to combine cyt c with membranes has to be taken into account. In this respect, the covalent conjugation of cyt c to carboxylated nanoparticles, provides a strong binding, leading to an improved stability for biosensing applications[58]. However, up to now, there is no report regarding the effect of combination strategies of cyt c with planar membranes to distinguish its accessibility and the resulting peroxidase-like activity at different membranes.

Towards this goal, we first explored the formation of lipid, polymer and hybrid monolayers at the air-water interface to determine the surface pressure at which densely packed films were formed, before transferring them onto silica wafers with the Langmuir-Blodgett method. Then, we characterized integrity, topography and morphology of resulting supported membranes before and after the combination with cyt c by AFM and confocal laser scanning microscopy (CLSM), respectively. QCM-D

was used to quantify the amount of cyt c combined with each type of planar membrane and how it affected the viscoelastic properties thus providing insights into the accessibility of cyt c. After combination with different membranes, we assessed indirectly the peroxidase-like activity of cyt c by an Amplex red (AR)-based fluorimetric assay. These different approaches to combine a protein with planar membranes together with the differences in the composition, morphology and properties of these planar membranes serve to indicate, which are the essential factors for equipping different membranes with proteins in order to produce of efficient “active “surfaces”.

Materials and methods

Materials

1,2-dipalmitoyl-sn-glycero-3-phosphocholine (DPPC) and 1,2-dipalmitoyl-sn-glycero-3-phosphoethanolamine-N-(lissamine rhodamine B sulfonyl) (ammonium salt), rhodamine B labeled DPPC, were purchased from Avanti Polar Lipids (Alabaster, AL). Cytochrome c from bovine heart (≥95%) was obtained from Sigma-Aldrich and reconstituted to a concentration of 500 µg/mL with phosphate buffer (PB) solution. The phosphate buffer was prepared by using the Na2HPO4•7H2O, and NaH2PO4 which were purchased from Sigma-Aldrich. N-(3-Dimethylaminopropyl)-N’-ethylcarbodiimide (EDC), sulfo-N-hydroxy-sulfosuccinimide sodium salt (sNHS) and all reported organic solvents were obtained from Sigma-Aldrich. The silica slides (Ultrapak 100 mm thin wafer box) were purchased from Entegris Inc. (Germany) and used for layer deposition.

Polymer synthesis

The amphiphilic diblock copolymer poly(dimethyl siloxane)$_{90}$-block-poly(2-methyl-2-oxazoline)$_{10}$ with a carboxylic functional group at the end of the hydrophilic domain (PDMS$_{90}$-b-PMOXA$_{10}$-COOH) was synthesized according to the following protocol: monocarbinol-functionalized PDMS-OH was

synthesized by anionic ring-opening polymerization of hexamethylcyclotrisiloxane and end-group modification with 2-allyloxyethanol. Afterwards, PDMS-OH was activated with trifluoromethanesulfonic anhydride and chain-extended by cationic ring-opening polymerization with 2-methyl-2-oxazoline monomer. Quenching with triethylamine/water in order to obtain hydroxy-functionalized PDMS-b-PMOXA-OH was followed by end-group modification with succinic anhydride, leading to the final carboxy-functionalized PDMS-b-PMOXA-COOH.

The molecular weight of the copolymer was estimated as 8400 g/mol by nuclear magnetic resonance (1H-NMR) (Figure S1A). The dispersity of the copolymer was 2.09 according to gel permeation chromatography (GPC) (Figure S1B). In order to confirm the presence of the COOH end group, Fourier-transform infrared spectroscopy (FTIR) was performed, showing the characteristic COOH stretching at 1730 cm^{-1} (Figure S1C).

Area-surface pressure isotherms

The area-dependent surface pressure isotherms of lipid, copolymer and mixtures of lipid and copolymer were measured by Langmuir Teflon mini-trough (KSV Instruments, Finland). The trough was equipped with two movable, computer-controlled Delrin barriers for variation of the area per molecule and a Wilhelmy plate made of filter paper for measuring the surface pressure. The trough and barriers were cleaned with high purity chloroform (HPLC grade, Sigma-Aldrich) and ethanol (≤99.8%, Fluka) before each measurement, and the trough was filled with ultrapure water. A fresh Wilhelmy paper was mounted and fully wetted with ultrapure water every time. The copolymer, lipid and hybrid mixtures in chloroform were diluted with chloroform to a concentration of 1 mg/mL. An aliquot was spread onto the ultraclean water subphase with a glass Hamilton microsyringe and left untouched for 10 min to allow for chloroform evaporation. Then, the lipid, copolymer or hybrid monolayers at the air-water

interface were compressed with a constant rate of 10 mm min^{-1}. During all measurements, a constant temperature of 23 °C was maintained. All reported data represent triplicate measurements.

Brewster angle microscopy

Brewster angle microscopy (BAM) experiments were performed with the EP3SW system (Nanofilm Technologie GmbH, Göttingen, Germany) equipped with a Nd:YAG laser (λ = 532 nm), a long distance objective (Nikon, 20×), and a monochrome CCD camera. The size of the BAM image corresponds to 220 × 250 μm^2, with a resolution of 1 μm. The microscope was installed over the KSV Langmuir trough equipped with two movable barriers that lead to a symmetrical compression. The BAM measurements were done in triplicate in order to obtain the best representation of the images.

Preparation of silica wafers

Silica wafers were cut into slides of 1 cm^2 that were rinsed with ethanol and dried. Before using, slides were placed in a UV ozone cleaner (Jelight Company Inc, Irvine, USA) for 20 min to remove contaminants from the surface. The cleaned slides were immediately used for layer deposition.

Langmuir-Blodgett transfer

The Langmuir monolayers formed at the air-water interface were deposited on the solid substrate (silica wafer or silicon dioxide sensor QSX 303 SiO_2) by a vertical dipping method. The dipping speed was 0.5 mm/min for downstroke and upstroke, maintaining the surface pressure at 35 mN/m. The bilayer films were transferred to the silica substrate by immersing the dipper downstroke for deposition of the first layer and lifting it upstroke for deposition of the second layer.

184 Confocal laser scanning microscopy

185 For confocal laser scanning microscopy (CLSM), 1-2 volume % of rhodamine B-labeled lipid (Liss Rhod
186 PE) was added to the lipid/copolymer mixture before the LB transfer to the solid support. The supported
187 hybrid bilayer was transferred to a glass slide and imaged within 1 h after the LB deposition. CLSM
188 images were recorded on a Zeiss 880 LSM equipped with a 40x water-immersion objective (C-
189 Apochromat 40x/1.2 W Korr FCS M27). A DBSS 561-10 laser (λ = 561 nm) with laser power at 2% was
190 used for the excitation of Liss Rhod PE. The fluorescence intensities of the images were analyzed by
191 ImageJ (v. 1.52r).

192

193 Atomic force microscopy

194 Atomic force microscopy (AFM) was performed with a JPK NanoWizard 3 AFM (JPK Instruments AG).
195 AC mode topography images were obtained in air, using silicon cantilevers (Tap150 Al-G, Budget
196 Sensors) with a nominal spring constant of 10−130 Nm^{-1} and a resonance frequency of 150 kHz. Images
197 were analyzed with the data analysis software JPK Data Processing (v. 5.0).

198

199 Quartz crystal microbalance with dissipation

200 Quartz crystal microbalance with dissipation (QCM-D) with Q-Sense E1 (Biolin Scientific, Sweden) set
201 up was employed to characterize the combination of cyt c to the membrane on silicon dioxide sensors.
202 Changes in the resonance frequency (ΔF) and energy dissipation (ΔD) of the oscillating sensor chip (QSX
203 303 SiO^2) as a function of time were simultaneously recorded at multiple odd overtones (3rd, 5th, 7th,
204 9th and 11th). All data shown represent recordings at the 7th overtone. In order to estimate the mass of
205 protein attached to the different membranes, the Sauerbrey equation was applied. This equation
206 converts the frequency shift into mass by using simple relation; $\Delta m = -C\Delta f$, where Δm is the mass, C is
207 the proportionality constant (17.7 ng cm^{-2} Hz^{-1}) and Δf is the frequency shift. After establishing a

baseline in aqueous buffer solution, QCM-D measurements were conducted under continuous flow conditions. A flow rate of 50 µL/min for protein addition and washing processes was delivered by a Reglo Digital peristaltic pump (Ismatec, Glattbrugg, Switzerland). The temperature of the flow cell was fixed at 24.0 ± 0.5 °C.

Activation of the carboxylic end group of copolymers in the membranes by EDC/NHS

For the covalent combination of cyt c to the copolymers in the solid-supported membranes, the functional carboxylic end groups were first activated to amine-reactive NHS esters by submerging the membranes in 3 mL of EDC solution (10 mg/ml in PB) for 10 min under gentle agitation. After washing with Phoshate buffer (PB) for 30 minutes to remove the unbound molecules, the membranes were submerged into sNHS solution (10 mg/ml in PB) for 10 min and washed again with buffer.

Fluorimetry

Fluorimetry was performed with a Spectramax M5e microplate and cuvette reader (Molecular Devices, USA) using a 10 mm light path quartz cuvette (Hellma, Germany), an excitation wavelength of 570 nm, and an emission wavelength of 595 nm. All specimens were measured immediately after QCM-D. The silica substrate was placed standing upright in the cuvette, facing the light source. Amplex red (AR) and H2O2 were added to a final concentration of 3.3 mM and 0.66 mM, respectively, and the final volume adjusted to 3 mL with 100 mM PB.

Results and Discussion

Monolayers at air-water interfaces

We measured the changes in the surface pressure of 1,2-dipalmitoyl-sn-glycero-3-phosphocholine (DPPC) lipid, PDMS90-b-PMOXA10-COOH copolymer and the mixture of both with weight ratio 50:50 wt. % as a function of the mean molecular area occupied by a molecule (Figure 1 A). Above the surface

pressure of 15 mN/m, all isotherms showed a transition from liquid expanded to liquid condensed phase, irrespective of the composition. Isotherm of PDMS90-b-PMOXA10-COOH copolymer showed a lift-off around 1750 Å, a larger plateau and a breaking point higher than 40 mN/m, indicating highly flexible monolayers at the air-water interface, already observed for other PMOXA-PDMS copolymers 38.Isotherm of the DPPC lipid exhibited a lift-off at circa 100 Å with a steep slope and a breaking point at 60 mN/m. Isotherm of the mixture of the DPPC lipid and $PDMS_{90}$-*b*-$PMOXA_{10}$-COOH copolymer, called hybrid, displayed an intermediate profile compared to the isotherms obtained from single components, with a lift-off lower than 1000 Å and a breaking point at 49 mN/m. During the recording of the Langmuir isotherms at air-water interface, the changes in morphology of the lipid, copolymer and hybrid monolayers were real-time monitored by BAM (Figure 1B). During the compression of the copolymers (Figure 1B (a-c)), lipids (Figure 1B (d-f)) and copolymers-lipids mixture (Figure 1B (g-i)) at three representative surface pressure (0, 9 and 35 mN/m, respectively). Initially, when no surface pressure was applied, no film was observed. At the surface pressure of 15 mN/m, the copolymers formed micelles at the air-water interface and then they changed their micellar architecture to a homogenous copolymer monolayer at the surface pressure of 35 mN/m (Figure 1B b-c), in agreement to previous reports for block copolymers[59]. In the case of lipids, flower like assemblies with sizes of approximately 10 µm were observed at a surface pressure of 9 mN/m, which transformed to planar lipid monolayers at air water interface for a surface pressure of 35 mN/m (Figure 1 e-f). The lipid-copolymer mixture did not show any assemblies at the intermediate surface pressure of 9 mN/m, and micron sized domains were observed at the surface pressure of 35 mN/m due to separation of lipids from the copolymers (Figure 1 h-i). It is important to mention that polymer-lipid phase separation does not completely occur, and each domain is not pure, presenting partially the other component. The lipid domains were found to be embedded into the continuous polymer rich phase, as already observed elsewhere12.

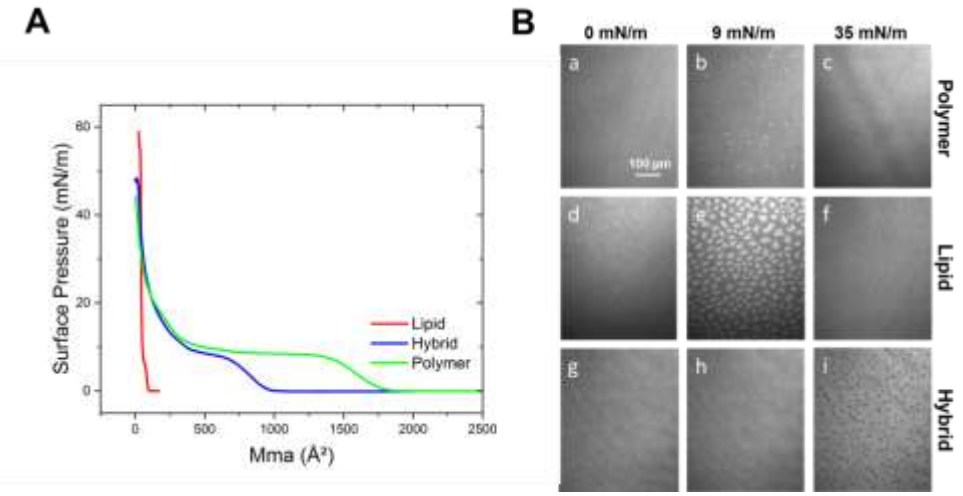

Figure 1. Langmuir isotherms of lipid, copolymer and hybrid (50:50 wt.%) (A) and BAM images of lipid, polymer and hybrid (B) at surface pressure of 0, 9 and 35 mN/m.

Formation of different model membranes on solid support

Monolayers of polymer, lipid and hybrid mixture were transferred to solid support using Langmuir Blodgett method, to create supported polymer, lipid and hybrid bilayer membranes, respectively. First, the monolayers at the air-water interface were deposited to the solid support through an upstroke at aconstant surface pressure of 35 mN/m [8, 17, 26, 60], resulting in solid-supported monolayers (Figure S2). AFM images showed that the solid-supported polymer monolayer was not homogenous and self-assembled into micellar structures with sizes of 20 nm on solid support, which is in agreement with literature reports (Figure S2A) [48, 61]. In contrast, the hybrid monolayer was uniform on solid support, with lipid and polymer domains, which had a height difference of 6-8 nm (Figure S2B). This difference was caused by the molecular mismatch between lipids and block copolymers.

The supported bilayer membranes were prepared by LB transferring, on a silica support, oftwo consecutive monolayers, one deposited via an upstroke and a following via a down-stroke[62]. The surface morphology and topography of the resulting bilayer membranes were analyzed by AFM phase

273 and height imaging (Figure 2). Phase profile was necessary to observe the domain separation, whereas

274 the height profile showed the mismatch between the polymer and the lipid phase domains in the hybrid

275 membranes. Surface topography of supported polymer membrane was planar and homogenous (Figure

276 2A and S3A), indicating that the deposition of a second layer induced the formation of a stable planar

277 architecture. After drying, there were no micellar structures on the supported polymer membranes, in

278 contrast to the polymer monolayer). As confirmed by AFM profiles, the supported DPPC lipid

279 membranes contained several defects (Figure 2B and S3B), due to the possible overturning mechanism

that occurred during the deposition[61]. Moreover, supported hybrid membranes showed clear separation of lipid and polymer domains (Figure 2C and S3C). The height difference between lipid and polymer domains in hybrid membrane was approximately of 11 ± 1 nm. The AFM phase image shows dark that represent the lipid domains and bright spots that represent the polymer domains. Domain enrichment was also observed: small polymer clusters were present in lipid-rich phase while small lipid clusters were present in polymer-rich domains. As the size of the lipid or polymer domains are tens of micron, there is no limit for size of proteins, which are either inserted or conjugated to the membranes as long as they

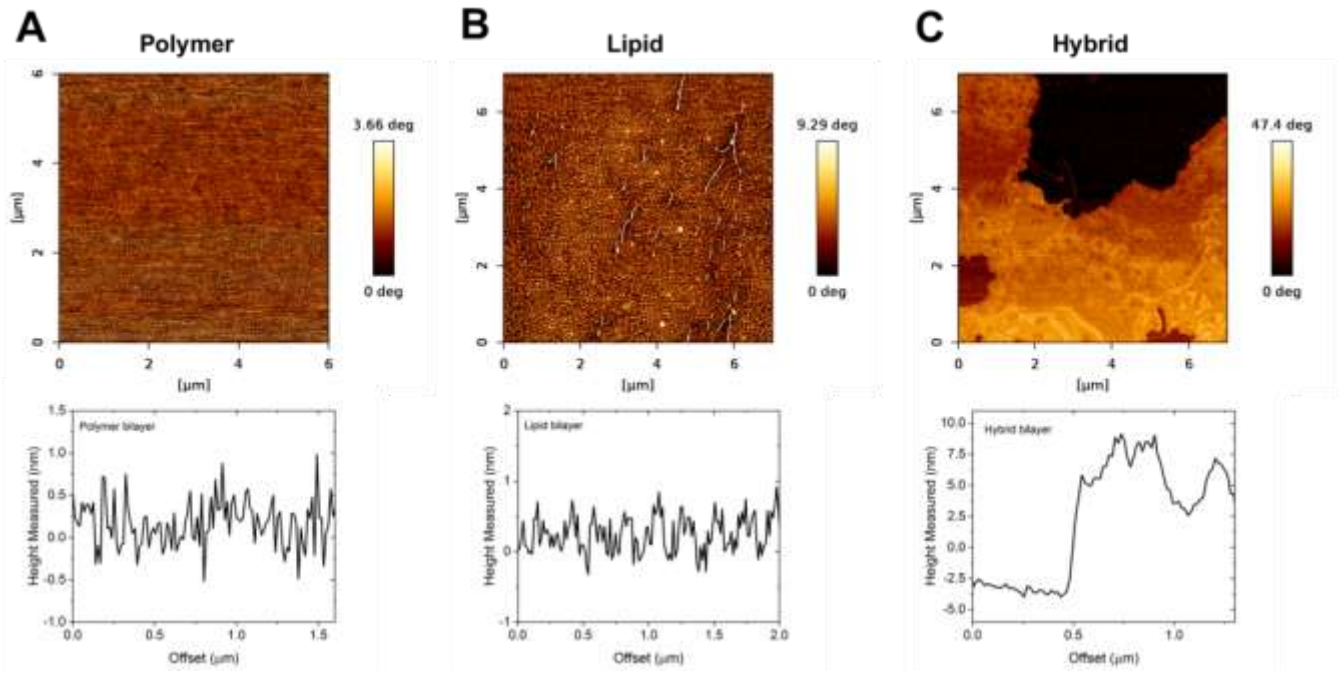

have specific characteristics (e.g. surface charge or hydrophobic part for insertion, functional group for conjugation). Therefore, any hydrophilic peripheral proteins can be inserted or conjugated to hybrid membranes after necessary adjustments of the membrane composition. For example, extracellular matrix (ECM) proteins (e.g. collagen with molecular weight of approximately 300 kDa or fibronectin with molecular weight of approximately 220 kDa) have been attached to the polymer domains through covalent conjugation and their effect on cell adhesion, proliferation and function have been investigated for development of cell-based diagnostics, tissue engineering, medical implants and biosensors[63].

Figure 2. AFM characterization of solid-supported bilayers. Phase profile (up) and cross section (down) of polymer (A), lipid (B) and hybrid (C) membranes. Corresponding height images are reported in Figure S3.

We then investigated the presence of lipid-rich or polymer-rich domains in hybrid bilayers, by CLSM (Figure S4A). Rhodamine B labelled lipid was added (1 wt. %) into the solution of the hybrid mixture before deposition onto silica support. The Rhodamine B lipid diffused only into the polymer-rich domains, as indicated by red colour, because they are both in a fluid phase. The blend of a small fraction of lipids with polymers into hybrid bilayers was due to similarity of the phases of the labeled lipid with the polymer. On the contrary, dark domains are specific for DPPC lipids, and are similar in shape and size when compared to BAM images[62, 64]. To further explore the uniformity of supported model membranes, we evaluated the adsorption of bovine serum albumin (BSA), a globular protein which has been previously used to determine membrane surface coverage[61-62, 64-65]. BSA adsorption was appreciable on silicon dioxide compared to the planar bilayer membranes made of DPPC lipids or PMOXA-PDMS copolymers[65]. In principle, BSA adsorption is expected to be negligible on the defect-free membranes deposited on silicon dioxide, whereas it increases with increasing amount of defects found in a membrane, e.g. the availability of bare silicon oxide for BSA. We quantified the BSA adsorption onto polymer, lipid and hybrid membranes by QCM-D and compared them with bare silicon dioxide support (Figure S5). A solution of BSA (C = 500 μg mL-1) was injected onto bare silica or supported membranes after baselines were established in PB. BSA adsorption on silicon dioxide led to a frequency shift of -24 ± 1 Hz whereas on supported polymer membrane of −2 ± 1 Hz which resulted in an appreciable reduction in amount of BSA adsorbed. We calculated a membrane surface coverage higher than 92 ± 4 %, indicating that the polymer membrane did not contain major defects. By contrast, the frequency shift

was −6 ± 2 Hz for the BSA adsorption on supported lipid membranes, leading to a reduction of membrane coverage to 75 ± 3 %. Thus, there were more defects in supported lipid membranes compared to hybrid or polymer counterparts. These results were in agreement with AFM data. In the case of BSA adsorption onto supported hybrid membranes, the frequency shift to −4 ± 2 Hz, was associated with a membrane surface coverage of 83 ± 4 %. The presence of defects on the membranes on silica was also compensated by covering the defects with BSA adsorption, which is expected to prevent nonspecific interactions of cyt c with bare silicon oxide.

Combination of cytochrome c with supported model membranes

After depositing the membranes, we monitored the real-time combination of cyt c with the lipid, polymer and hybrid membranes. We employed two different strategies: i) cyt c insertion into the membrane through hydrophobic interactions, and ii) covalent conjugation (Figure 3) of cyt c to the membranes by binding the accessible lysine of cyt c to COOH functionalized polymer through EDS/sNHS coupling chemistry[52, 66-67]. The conjugation provides stability to cyt c, preventing the loss of its heme or denaturation. Because cyt c is normally found in the inner cell membranes, the covalent bond provides the needed stability for cyt c when located on the outer membrane[67-68].

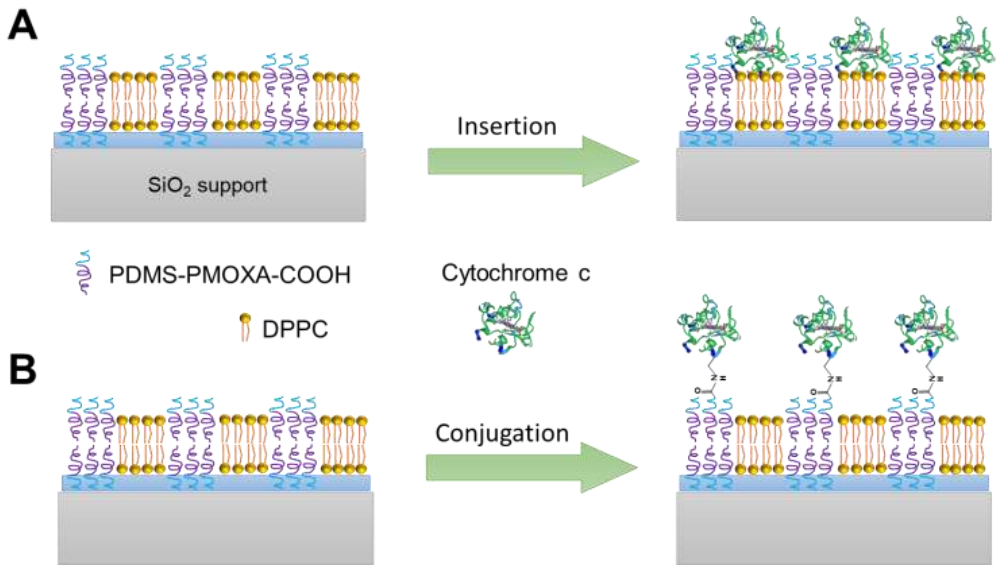

Figure 3. Schematic representation of hybrid supported bilayer and their combination with model protein cytochrome c through (A) insertion and (B) covalent conjugation by EDC/sNHS coupling.

We compared the insertion of cyt c into solid supported membranes by QCM-D (Figure 4A). The QCM-D measurement baseline signals were stabilized in phosphate buffer. After 5 min of baseline stabilization, a solution of 500 µg/ml of cyt c was injected. First, we monitored cyt c combination onto silica surface (Figure S6), resulting in a frequency shift of -16.4 ± 5.8 Hz and a cyt c mass of 290 ± 103 ng/cm^2. The combination here consisted in an irreversible and not selective process, since it was driven by either attractive electrostatic interaction between positively charged cyt c and negatively charged silica and , which could result in protein denaturation. Moreover, cyt c insertion into supported polymer and hybrid membranes led to a similar frequency shift of -8.0 ± 0.9 Hz and -7.5± 2.1 Hz, respectively, while it led to small frequency shift of -2.4± 2.3 Hz for the supported lipid membranes. The mass of the inserted cyt c was estimated by using the Sauerbrey equation (Table 1). The mass of inserted cyt c on the supported polymer bilayer was 142 ± 16 ng/cm^2, 133 ± 38 ng/cm^2 for hybrid bilayer and only 42 ± 40 ng/cm^2 for lipid bilayer. The frequency shifts obtained from cyt c adsorption in the presence of polymer-, lipid- and hybrid-based layers were lower than the one obtained from bare silica substrate because PMOXA-PDMS block copolymer has antifouling characteristics and cyt c combination was driven by specific interactions[69].

Table 1. Quantification of cytochrome c combined with polymer and hybrid membranes

Membrane type	Frequency Shift[a]		Mass[a]		Molecules of cyt c	
	Insertion	Conjugation	Insertion	Conjugation	Insertion	Conjugation

Polymer	-8.0 ± 0.9	-7.4 ± 0.8	142 ± 16	132 ± 18	7.1 ± 0.8	6.6 ± 0.7
Hybrid	-7.5 ± 2.1	-2.5 ± 0.7	133 ± 38	44 ± 13	6.7 ± 1.9	2.2 ± 0.6
Lipid	-2.4 ± 2.3	n.a.[b]	42 ± 40	n.a.	2.1 ± 2.0	n.a.

[a]The Frequency is reported in Hz, the mass is reported in ng/cm^2, the molecules of cyt c have to be multiplied by 10^{12}. [b]Not available, the conjugation was not performed for the lipid because it has no carboxylic end group. The quantity of cyt c combined with the two strategies are compared.

To gain more insight into the viscoelastic properties of the combined cyt c on the different supported membranes, we used the correlation between dissipation and frequency (Figure 4B), which can be linked to accessibility of the protein on the membrane surface[70]. The dissipation value for the lipid membrane was around $0.1*10^{-6}$ and lower than the value determined for the polymer and hybrid membranes ($0.7*10^{-6}$ and $0.5*10^{-6}$, respectively). The values for dissipation also indicate the difference in the overall flexibility of the different membranes: polymer and hybrid membranes present a higher degree of mobility due to their molecular structure and the resulting membrane packing, compared to lipid membrane 12. This is in agreement with the fact that the lipid is in the gel phase. Secondly, the cyt c was covalently conjugated to supported polymer bilayer and hybrid bilayer, based on the formation of a peptidic bond between the ending functional group of the functionalized polymer and the outer lysine of the cyt c (Figure S7)[52].

The conjugation reaction was performed before the addition of cyt c to the bilayers. The carboxylic groups of the polymers were activated by injecting EDC/sNHS solution (C = 10 mg/ml) (Table S1) and then rinsed with buffer, before the injection of cyt c solution (C = 500 µg/ml). Nevertheless, during the conjugation reaction a small amount of cyt c may have also inserted into the membrane. The conjugation of cyt c to the supported polymer bilayer led to a frequency shift of -7.4 ± 0.8 resulting in a mass of 132 ± 18 ng/cm^2, while the conjugation of cyt c to the supported hybrid bilayer induced a

frequency shift of -2.5 ± 0.7 Hz, resulting in a mass of 44 ± 13 ng/cm^2 (Table 1). The lower amount of cyt c conjugated to the hybrid membrane is mainly due to the lower number of carboxylic groups available compared to the polymer membrane, according to the molar ratio of 50% in the hybrid. No conjugation was performed for the lipid membrane, due to the absence of the carboxylic functionalization. When we compared the two combination strategies of cyt c for the supported hybrid bilayers, the frequency shifts for the insertion method was higher than for the conjugation (Figure 4C), while the dissipation shifts revealed to be higher for the conjugation, with the highest value of $1.0*10^{-6}$ (Figure 4D). The differences in the frequency/dissipation ratio suggest that cyt c has a different conformation when it is combined with the hybrid bilayers by using different combination strategies. The explanation relies on the higher degree of freedom cyt c has when it is conjugated to the membrane, standing away from it, instead of partially penetrating it with its hydrophobic part. Moreover, cyt c preferred a combination with the hybrid membrane through insertion rather than conjugation. However, neutral DPPC lipid cannot establish a strong attractive electrostatic interaction with the positive-charged cyt c. Instead, the presence of anionic lipids in the hybrid membrane may increase the insertion of the protein[48, 71-74]. The isoelectric point (pI) of cyt c is in the range of 10.0-10.5 and in condition of neutrality it presents a positive charge[52], so by increasing the pH over this value it would be possible to inhibit the spontaneous insertion due to repulsive interactions between the membrane and the protein[52]. We kept here the system at neutral pH condition.

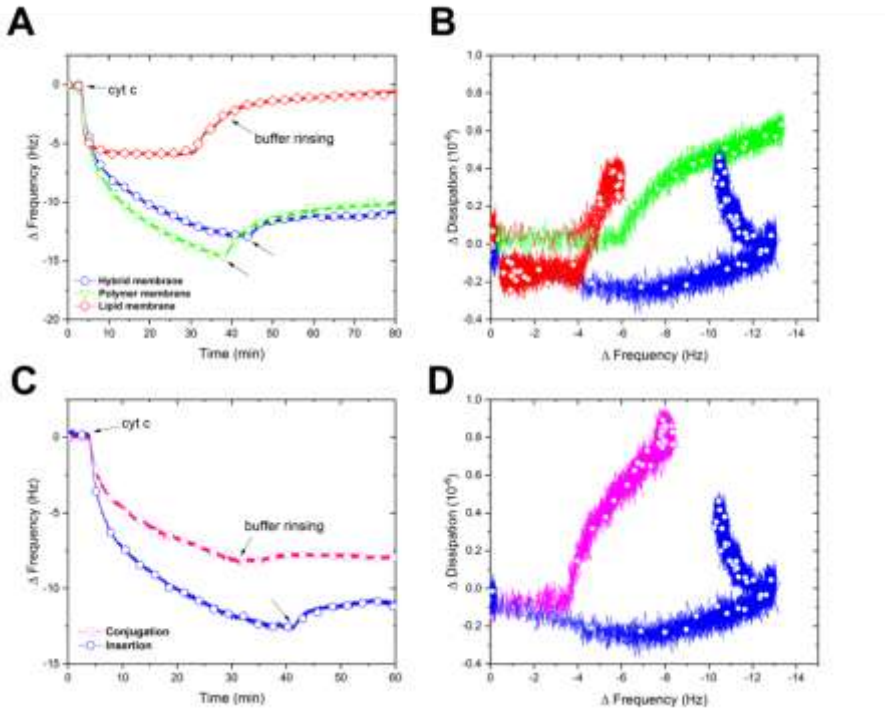

Figure 4. QCM-D plots of protein combination with supported membranes: protein insertion (A); comparison of protein combination methods with hybrid membrane (C) and their corresponding ΔD vs Δf plots (B and D). Solutions used are cytochrome c in PB (500 µg/ml) and pure PB for rinsing steps.

After insertion of cyt c within the different membranes, we also monitored the changes in membrane integrity by analysing AFM height and phase profiles. Because of the small size of cyt c (approximately 3 nm) compared to the domain sizes, we assume that each domain can accommodate more than one cyt c. After the protein insertion, we observed that, in general, the protein aggregates in clusters (white spots) of different sizes and average height of 5 ± 2 nm. No modification of the polymer membrane architecture was observed after cyt c insertion: the synthetic membranes preserved their planarity and homogeneity, probably due to their robustness (Figure S8B). The low cyt c height (2 ± 1 nm) found in polymer membrane, might be due to a deeper penetration of the protein into the bilayer, as compared to lipid and hybrid membranes (Figure 5A). As the lipid bilayer was removed from the silica support,

similarly to other reports[48, 57], it resulted in a discontinuous membrane (Figure S8A) with cyt c clusters mainly located on the silica dark background (Figure 5B). Desorption of lipid bilayers from the silica after addition of cyt c was also confirmed by QCM-D (Figure 4A): the decrease in mass observed before the buffer-rinsing step indicated the removal of the membrane from the support. Interestingly, the interaction of the cyt c with the hybrid bilayer indicated no bilayer removal, as expected for the lipid phase, rather a bilayer reorganization took place, where the lipids self-assembled in the polymer matrix and constituted rafts accommodating the protein (Figure 5C and S9). The copolymer preserved the bilayer integrity due to its mechanical resistance while the lipid phase allowed the cyt c to insert due to its fluidity[22, 75]. Therefore, the hybrid bilayer was suitable for achieving a selective combination of the protein with a specific bilayer domain: the lipid domain allowed the insertion while the polymer one served for the conjugation.

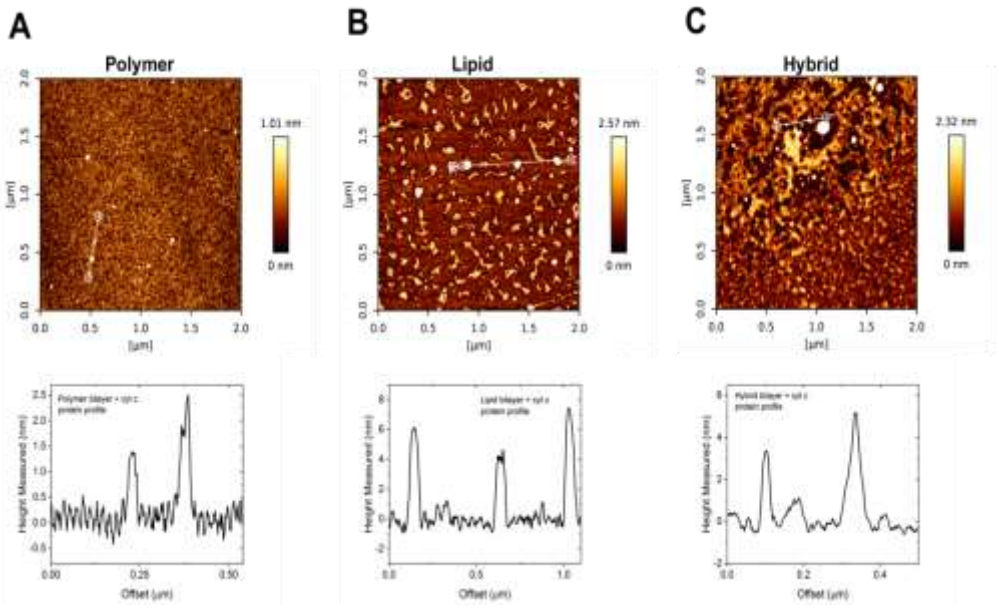

Figure 5. AFM height profile of different membranes after protein insertion: polymer (A), lipid (B) and hybrid bilayers (C).

Assessment of peroxidase-like activity of cyt c on supported hybrid membranes

Cyt c plays an important role in the elimination of hydrogen peroxide (H_2O_2) from mitochondria and respiratory chain, leading to exhibited peroxidise-like activity[76]. The activity of cyt c is based on the reaction of its iron (III) porphyrin, which, in the presence of a cofactor, turns to an oxo-iron species that rapidly oxidize different substrates[77]. We evaluated the peroxidase-like activity of cyt c when combined with supported polymer and hybrid bilayers either by two different combination approaches: i) insertion or ii) conjugation. We did not evaluated solid-supported lipid membranes due to their instability after insertion of cyt c. We assessed indirectly the cyt c activity in the presence of the cofactor H_2O_2, with an Amplex red (AR) based fluorimetric assay. This colorless, non-fluorescent substrate can be oxidized by the $OH^{\cdot}$ radicals, produced by cyt c, to the colored and fluorescent resorufin (Figure S10A). A first indication of a successful reaction was the color change of the solution (Figure S10B and S10C). Time-dependent kinetics of resorufin fluorescence intensity (in arbitrary units, a.u.) induced by the addition of H_2O_2 to cyt c serves to evaluate the peroxidase-like activity of cyt c after its combination with supported polymer and hybrid membranes (Figure 6). In order to eliminate the effects of amplex red auto-oxidation from the spontaneous dissociation of H_2O_2 and avoid overestimating the peroxidase-like activity of cyt c, we used the AR auto-oxidation for background correction. We did not expect a degradation of hybrid membranes by the presence of H_2O_2, as experiments in similar conditions have been already tested for PDMS-b-PMOXA polymers , resulting that no significant membrane disturbance by H_2O_2 were observed[78-79]. Moreover, a negligible oxidation of AR by H_2O_2 was observed by the fluorometric measurements and AR here served as a scavenger and prevented a possible degradation of lipid domains. The activity of cyt c when combined with polymer or hybrid membranes, was always preserved in different degrees as compared with the free protein (Figure 6A), regardless from the combination method adopted. As expected, cyt c has a lower activity, which can be explained by two factors: i) a reduced conformational freedom of cyt c due to its interaction with the membrane, and ii) the fact that the enzyme only covers a bidimensional space, to which the substrates must diffuse,

instead of occupying the entire volume, underlying that diffusion is a fundamental parameter[79]. Besides, the presence of molecules nearby the bilayer interface, might cause further oxidation of the produced resorufin, before it diffuses back into the bulk of the solution, to non-fluorescent dihydroresazurin[80-81], inducing a drop in the fluorescence signal detected in the initial non-linear kinetics. When the cyt c was covalently bound to supported polymer or hybrid membranes, a higher peroxidase-like activity was determined, compared to cyt c inserted into the membranes. This is due to a higher accessibility of the protein for the substrates when it is conjugated. When cyt c is inserted, a greater density of cyt c on the membrane than the previous case (per QCM-D measurements) does not translate into higher activity, likely because such technique does not ensure an easy accessibility of the enzyme's active site, which can end up buried towards the membrane, whereas the anchoring of cyt c prevents it from inserting with a wrong orientation[82]. Moreover, QCM-D overestimates the density of cyt c on the membranes since bound water was also taken into account when calculating the protein density. Therefore, when the bound water is subtracted, actual density of cyt c on the membranes might be smaller and directly correlated with activity. In order to obtain a rough estimation of the average activity of the protein, inserted and conjugated into polymer and hybrid membranes, the intensity of fluorescence after 10 minutes was normalized by the number of cyt c molecules. It was found that cyt c inserted into the polymer membrane exhibits a low activity, with a fluorescence intensity of 30 a.u. The value slightly increased for the cyt c inserted into the hybrid membrane (50 a.u.). A high activity was instead found for the cyt c conjugated to the hybrid membrane, with the highest value of circa 300 a.u. Remarkably, in both cases the activity was increased if the protein was associated to a hybrid membrane, rather than the purely polymeric one, in this case the presence of lipid rafts might play an important role, increasing the flexibility of the protein and the mobility within the membrane and, consequently, improving its accessibility. To study the long-term activity of our hybrid membranes, we followed the enzymatic oxidation of Amplex red for 12 h, for inserted and conjugated cyt c (Figure 6B). Even though the

intensity profile is similar within the first 200 minutes, afterwards the activity of the conjugated cyt c drifts to higher values than the inserted cyt c, confirming the sustained and long-lasting activity of the protein with a proper accessibility. Further studies will evaluate in more details cyt c after insertion or conjugation with the hybrid membrane.

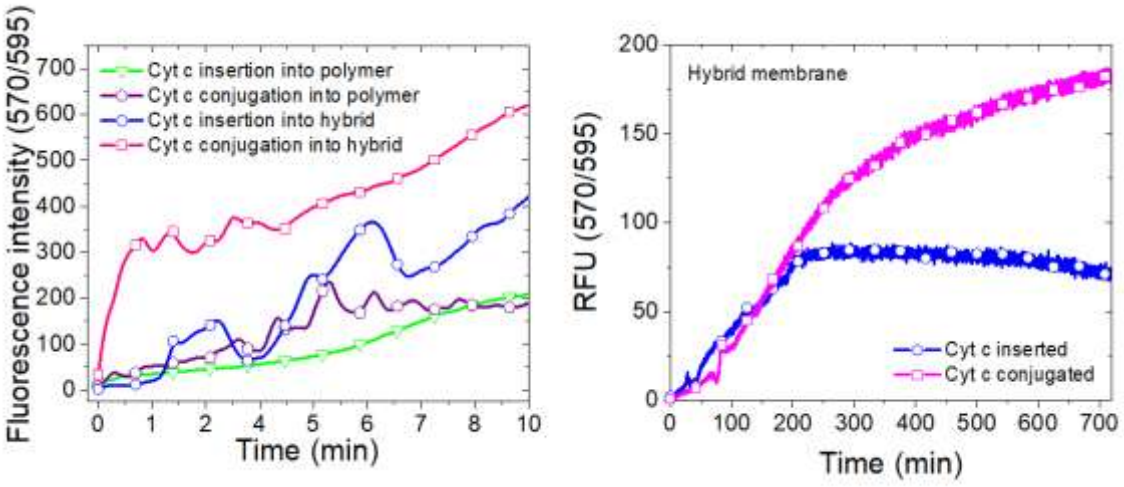

Figure 6. Qualitative comparison of protein activity by fluorimetric assay after the combination with different membranes for 10 minutes (A), and with hybrid membrane through different methods for 12 hours (B).

Conclusions

The combination of artificial planar membranes with biomolecules has high potential for development of efficient active surfaces where the functionality is given by the specificity of the biomolecules. Depending on the combination strategy adopted, it is possible to tune the protein distribution into a specific domain of hybrid membranes (polymer- or lipid-rich phase). Here we utilised two strategies – insertion and conjugation – for combining the peripheral membrane protein cyt c with a specific domain of the hybrid membranes based on mixture of PDMS-*b*-PMOXA diblock copolymers and DPPC lipid. The lipid in the hybrid membrane preferentially promoted the cyt c insertion into lipid domains, while the

copolymer allowed the conjugation with the cyt c into polymer domains through the carboxylic functionalization. The comparison between the hybrid and one-component membranes (e.g. polymer or lipid) revealed that the protein activity was higher in hybrid membranes, due to the combined properties of lipid and polymer. Moreover, the conjugation strategy resulted as the best approach for increasing the cyt c accessibility and stability, and consequently its activity. Our results open the possibility to extend the combination to different proteins, as for example Horseradish peroxidase (HRP), after proper adaption of the system. Taken together, our results support further development of complex and versatile hybrid bio-interfaces by indicating the molecular factors that are relevant when biomolecules are combined with planar synthetic membranes, especially when they are hybrid and thus contain both lipid- and polymer domains.

TABLE OF CONTENT

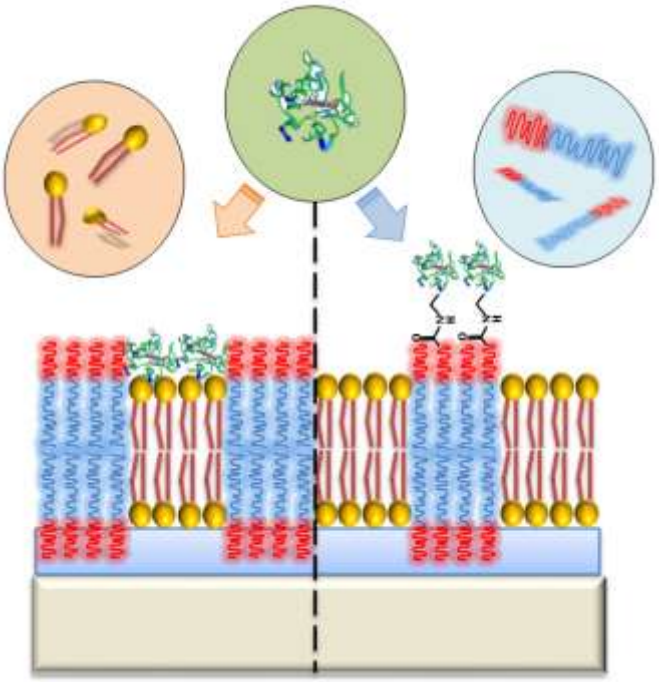

ASSOCIATED CONTENT

Supporting Information

Characterization of PDMS-*b*-PMOXA diblock copolymer with NMR, FTIR and GPC; schematic representation of protein conjugation strategy; AFM images of polymer mono and bilayer, hybrid and lipid bilayer after protein combination; Schematic representation of protein-bilayer conjugation; QCM data for quantification of EDC/sNHS conjugation for comparison of protein combination with and without BSA step; and comparison of polymer and fluorimetry study for protein activity.

ACKNOLEDGMENT

We acknowledge the Swiss Nanoscience Institute, the Swiss National Science Foundation, the NCCR Molecular System Engineering and the University of Basel for financial support. SDL thanks Swiss Nanoscience Institute for his PhD grant. Dr. Dalin Wu (University of Basel) is thanked for copolymer synthesis and fruitful discussions. Dr. Ioana Craciun and Dr. Cora-Ann Schönenberger (University of Basel) are acknowledged for editing the manuscript and useful discussions.

REFERENCES

1. Sackmann, E. Biological membranes architecture and function. *Structure and Dynamics of Membranes* **1995,** *1*, 1-63.
2. Gust, D.; Moore, T. A.; Moore, A. L. Mimicking photosynthetic solar energy transduction. *Accounts of Chemical Research* **2001,** *34* (1), 40-48.
3. Lin, Q.; London, E. Preparation of artificial plasma membrane mimicking vesicles with lipid asymmetry. *PloS one* **2014,** *9* (1).
4. Steinberg-Yfrach, G.; Rigaud, J.-L.; Durantini, E. N.; Moore, A. L.; Gust, D.; Moore, T. A. Light-driven production of ATP catalysed by F 0 F 1-ATP synthase in an artificial photosynthetic membrane. *Nature* **1998,** *392* (6675), 479-482.
5. Castellana, E. T.; Cremer, P. S. Solid supported lipid bilayers: From biophysical studies to sensor design. *Surface Science Reports* **2006,** *61* (10), 429-444.
6. Vockenroth, I. K.; Atanasova, P. P.; Jenkins, A. T. A.; Koeper, I. Incorporation of α-hemolysin in different tethered bilayer lipid membrane architectures. *Langmuir* **2008,** *24* (2), 496-502.
7. Kowal, J. Ł.; Kowal, J. K.; Wu, D.; Stahlberg, H.; Palivan, C. G.; Meier, W. P. Functional surface engineering by nucleotide-modulated potassium channel insertion into polymer membranes attached to solid supports. *Biomaterials* **2014,** *35* (26), 7286-7294.

8. Draghici, C.; Kowal, J.; Darjan, A.; Meier, W.; Palivan, C. G. “Active Surfaces” Formed by Immobilization of Enzymes on Solid-Supported Polymer Membranes. *Langmuir* **2014,** *30* (39), 11660-11669.
9. Sackmann, E. Supported membranes: scientific and practical applications. *Science* **1996,** *271* (5245), 43-48.
10. Belluati, A.; Mikhalevich, V.; Yorulmaz Avsar, S.; Daubian, D.; Craciun, I.; Chami, M.; Meier, W. P.; Palivan, C. G. How do the properties of amphiphilic polymer membranes influence the functional insertion of peptide pores? *Biomacromolecules* **2019**.
11. Dahlin, A.; Zäch, M.; Rindzevicius, T.; Käll, M.; Sutherland, D. S.; Höök, F. Localized surface plasmon resonance sensing of lipid-membrane-mediated biorecognition events. *Journal of the American Chemical Society* **2005,** *127* (14), 5043-5048.
12. Kowal, J.; Wu, D.; Mikhalevich, V.; Palivan, C. G.; Meier, W. Hybrid polymer–lipid films as platforms for directed membrane protein insertion. *Langmuir* **2015,** *31* (17), 4868-4877.
13. El Idrissi, M.; Meyer, C. E.; Zartner, L.; Meier, W. Nanosensors based on polymer vesicles and planar membranes: a short review. *Journal of nanobiotechnology* **2018,** *16* (1), 1-14.
14. Gettel, D. L.; Sanborn, J.; Patel, M. A.; de Hoog, H.-P.; Liedberg, B.; Nallani, M.; Parikh, A. N. Mixing, diffusion, and percolation in binary supported membranes containing mixtures of lipids and amphiphilic block copolymers. *Journal of the American Chemical Society* **2014,** *136* (29), 10186-10189.
15. Schulz, M.; Olubummo, A.; Bacia, K.; Binder, W. H. Lateral surface engineering of hybrid lipid–BCP vesicles and selective nanoparticle embedding. *Soft Matter* **2014,** *10* (6), 831-839.
16. Schulz, M.; Werner, S.; Bacia, K.; Binder, W. H. Controlling molecular recognition with lipid/polymer domains in vesicle membranes. *Angewandte Chemie International Edition* **2013,** *52* (6), 1829-1833.
17. Discher, D. E.; Eisenberg, A. Polymer vesicles. *Science* **2002,** *297* (5583), 967-973.
18. Morigaki, K.; Kiyosue, K.; Taguchi, T. Micropatterned composite membranes of polymerized and fluid lipid bilayers. *Langmuir* **2004,** *20* (18), 7729-7735.
19. Palivan, C. G.; Goers, R.; Najer, A.; Zhang, X.; Car, A.; Meier, W. Bioinspired polymer vesicles and membranes for biological and medical applications. *Chemical society reviews* **2016,** *45* (2), 377-411.
20. Mashaghi, S.; van Oijen, A. M. A versatile approach to the generation of fluid supported lipid bilayers and its applications. *Biotechnology and bioengineering* **2014,** *111* (10), 2076-2081.
21. Kita-Tokarczyk, K.; Itel, F.; Grzelakowski, M.; Egli, S.; Rossbach, P.; Meier, W. Monolayer interactions between lipids and amphiphilic block copolymers. *Langmuir* **2009,** *25* (17), 9847-9856.
22. Hu, S.-W.; Huang, C.-Y.; Tsao, H.-K.; Sheng, Y.-J. Hybrid membranes of lipids and diblock copolymers: From homogeneity to rafts to phase separation. *Physical Review E* **2019,** *99* (1), 012403.
23. Chemin, M.; Brun, P.-M.; Lecommandoux, S.; Sandre, O.; Le Meins, J.-F. Hybrid polymer/lipid vesicles: fine control of the lipid and polymer distribution in the binary membrane. *Soft Matter* **2012,** *8* (10), 2867-2874.
24. Nam, J.; Vanderlick, T. K.; Beales, P. A. Formation and dissolution of phospholipid domains with varying textures in hybrid lipo-polymersomes. *Soft Matter* **2012,** *8* (30), 7982-7988.
25. Paxton, W. F.; McAninch, P. T.; Achyuthan, K. E.; Shin, S. H. R.; Monteith, H. L. Monitoring and modulating ion traffic in hybrid lipid/polymer vesicles. *Colloids and Surfaces B: Biointerfaces* **2017,** *159*, 268-276.
26. Haefele, T.; Kita-Tokarczyk, K.; Meier, W. Phase behavior of mixed Langmuir monolayers from amphiphilic block copolymers and an antimicrobial peptide. *Langmuir* **2006,** *22* (3), 1164-1172.
27. Amado, E.; Blume, A.; Kressler, J. Novel non-ionic block copolymers tailored for interactions with phospholipids. *Reactive and Functional Polymers* **2009,** *69* (7), 450-456.

28. Chimisso, V.; Maffeis, V.; Hürlimann, D.; Palivan, C. G.; Meier, W. Self-Assembled Polymeric Membranes and Nanoassemblies on Surfaces: Preparation, Characterization, and Current Applications. *Macromolecular Bioscience* **2020,** *20* (1), 1900257.
29. Richter, R.; Mukhopadhyay, A.; Brisson, A. Pathways of lipid vesicle deposition on solid surfaces: a combined QCM-D and AFM study. *Biophysical journal* **2003,** *85* (5), 3035-3047.
30. Jagoda, A.; Ketikidis, P.; Zinn, M.; Meier, W.; Kita-Tokarczyk, K. Interactions of Biodegradable Poly ([R]-3-hydroxy-10-undecenoate) with 1, 2-Dioleoyl-sn-glycero-3-phosphocholine Lipid: A Monolayer Study. *Langmuir* **2011,** *27* (17), 10878-10885.
31. Mathé, C.; Devineau, S.; Aude, J.-C.; Lagniel, G.; Chédin, S.; Legros, V.; Mathon, M.-H.; Renault, J.-P.; Pin, S.; Boulard, Y. Structural determinants for protein adsorption/non-adsorption to silica surface. *PloS one* **2013,** *8* (11).
32. Nakanishi, K.; Sakiyama, T.; Imamura, K. On the adsorption of proteins on solid surfaces, a common but very complicated phenomenon. *Journal of bioscience and bioengineering* **2001,** *91* (3), 233-244.
33. Rezwan, K.; Meier, L. P.; Gauckler, L. J. Lysozyme and bovine serum albumin adsorption on uncoated silica and AlOOH-coated silica particles: the influence of positively and negatively charged oxide surface coatings. *Biomaterials* **2005,** *26* (21), 4351-4357.
34. Ying, P.; Viana, A. S.; Abrantes, L. M.; Jin, G. Adsorption of human serum albumin onto gold: a combined electrochemical and ellipsometric study. *Journal of colloid and interface science* **2004,** *279* (1), 95-99.
35. Kim, D. T.; Blanch, H. W.; Radke, C. J. Direct imaging of lysozyme adsorption onto mica by atomic force microscopy. *Langmuir* **2002,** *18* (15), 5841-5850.
36. Hinnen, C. Electrochemical and spectroreflectance studies of the adsorbed horse heart cytochrome c and cytochrome CD3 from D. Vulgaris, Miyazaki Strain, at gold electrode. **1983**.
37. Reed, D. E.; Hawkridge, F. M. Direct electron transfer reactions of cytochrome c at silver electrodes. *Analytical chemistry* **1987,** *59* (19), 2334-2339.
38. Wang, L.; Wang, E. Direct electron transfer between cytochrome c and a gold nanoparticles modified electrode. *Electrochemistry Communications* **2004,** *6* (1), 49-54.
39. Patila, M.; Pavlidis, I. V.; Diamanti, E. K.; Katapodis, P.; Gournis, D.; Stamatis, H. Enhancement of cytochrome c catalytic behaviour by affecting the heme environment using functionalized carbon-based nanomaterials. *Process Biochemistry* **2013,** *48* (7), 1010-1017.
40. Tanne, J.; Dietzel, B.; Scheller, F.; Bier, F. Nanohybrid Materials Consisting of Poly [(3-aminobenzoic acid)-co-(3-aminobenzenesulfonic acid)-co-aniline] and Multiwalled Carbon Nanotubes for Immobilization of Redox Active Cytochrome c. *Electroanalysis* **2014,** *26* (4), 732-738.
41. Song, Y.; Liu, H.; Wan, L.; Wang, Y.; Hou, H.; Wang, L. Direct Electrochemistry of Cytochrome c Based on Poly (diallyldimethylammonium Chloride)-Graphene Nanosheets/Gold Nanoparticles Hybrid Nanocomposites and Its Biosensing. *Electroanalysis* **2013,** *25* (6), 1400-1409.
42. Eguilaz, M.; Agüí, L.; Yanez-Sedeno, P.; Pingarron, J. A biosensor based on cytochrome c immobilization on a poly-3-methylthiophene/multi-walled carbon nanotubes hybrid-modified electrode. Application to the electrochemical determination of nitrite. *Journal of Electroanalytical Chemistry* **2010,** *644* (1), 30-35.
43. Wang, Y.; Bian, X.; Liao, L.; Zhu, J.; Guo, K.; Kong, J.; Liu, B. Electrochemistry and biosensing activity of cytochrome c immobilized on a mesoporous interface assembled from carbon nanospheres. *Microchimica Acta* **2012,** *178* (3-4), 277-283.
44. Petrov, P.; Stassin, F.; Pagnoulle, C.; Jérôme, R. Noncovalent functionalization of multi-walled carbon nanotubes by pyrene containing polymers. *Chemical communications* **2003,** (23), 2904-2905.
45. Wu, J.-F.; Xu, M.-Q.; Zhao, G.-C. Graphene-based modified electrode for the direct electron transfer of cytochrome c and biosensing. *Electrochemistry Communications* **2010,** *12* (1), 175-177.

46. Salamon, Z.; Tollin, G. Reduction of cytochrome c at a lipid bilayer modified electrode. *Bioelectrochemistry and bioenergetics* **1991,** *25* (3), 447-454.
47. Salamon, Z.; Tollin, G. Interfacial electrochemistry of cytochrome c at a lipid bilayer modified electrode: effect of incorporation of negative charges into the bilayer on cyclic voltammetric parameters. *Journal of Electroanalytical Chemistry and Interfacial Electrochemistry* **1991,** *321* (2), 321-334.
48. Choi, E. J.; Dimitriadis, E. K. Cytochrome c adsorption to supported, anionic lipid bilayers studied via atomic force microscopy. *Biophysical journal* **2004,** *87* (5), 3234-3241.
49. Salamon, Z.; Tollin, G. Interaction of horse heart cytochrome c with lipid bilayer membranes: effects on redox potentials. *Journal of bioenergetics and biomembranes* **1997,** *29* (3), 211-221.
50. Tuominen, E. K.; Wallace, C. J.; Kinnunen, P. K. Phospholipid-cytochrome c interaction evidence for the extended lipid anchorage. *Journal of Biological Chemistry* **2002,** *277* (11), 8822-8826.
51. Gouveia, A.; Bajwa, E.; Klegeris, A. Extracellular cytochrome c as an intercellular signaling molecule regulating microglial functions. *Biochimica et Biophysica Acta (BBA)-General Subjects* **2017,** *1861* (9), 2274-2281.
52. Tuominen, E. K. Phospholipid–cytochrome c interactions. **2011**.
53. Salamon, Z.; Tollin, G. Surface plasmon resonance studies of complex formation between cytochrome c and bovine cytochrome c oxidase incorporated into a supported planar lipid bilayer. I. Binding of cytochrome c to cardiolipin/phosphatidylcholine membranes in the absence of oxidase. *Biophysical journal* **1996,** *71* (2), 848-857.
54. Kalanxhi, E.; Wallace, C. J. Cytochrome c impaled: investigation of the extended lipid anchorage of a soluble protein to mitochondrial membrane models. *Biochemical Journal* **2007,** *407* (2), 179-187.
55. Santucci, R.; Sinibaldi, F.; Fiorucci, L. Human Diseases and Mitochondrial Damage: Role of Cytochrome c–Cardiolipin Interaction as a Key Regulator of Cell Fate. *Frontiers in Medicinal Chemistry* **2016,** *9*, 56.
56. Boussaad, S.; Pean, J.; Tao, N. High-resolution multiwavelength surface plasmon resonance spectroscopy for probing conformational and electronic changes in redox proteins. *Analytical chemistry* **2000,** *72* (1), 222-226.
57. Morandat, S.; El Kirat, K. Real-time atomic force microscopy reveals cytochrome c-induced alterations in neutral lipid bilayers. *Langmuir* **2007,** *23* (22), 10929-10932.
58. Bayraktar, H.; You, C.-C.; Rotello, V. M.; Knapp, M. J. Facial control of nanoparticle binding to cytochrome c. *Journal of the American Chemical Society* **2007,** *129* (10), 2732-2733.
59. Kowal, J.; Zhang, X.; Dinu, I. A.; Palivan, C. G.; Meier, W. Planar biomimetic membranes based on amphiphilic block copolymers. ACS Publications: 2014.
60. Schwartz, D. K. Langmuir-Blodgett film structure. *Surface Science Reports* **1997,** *27* (7-8), 245-334.
61. Honig, E. Molecular constitution of X-and Y-type Langmuir-Blodgett films. *Journal of Colloid and Interface Science* **1973,** *43* (1), 66-72.
62. Draghici, C.; Mikhalevich, V.; Gunkel-Grabole, G.; Kowal, J.; Meier, W.; Palivan, C. G. Biomimetic planar polymer membranes decorated with enzymes as functional surfaces. *Langmuir* **2018,** *34* (30), 9015-9024.
63. Vafaei, S.; Tabaei, S. R.; Cho, N.-J. Optimizing the performance of supported lipid bilayers as cell culture platforms based on extracellular matrix functionalization. *ACS omega* **2017,** *2* (6), 2395-2404.
64. Itel, F.; Chami, M.; Najer, A.; Lörcher, S.; Wu, D.; Dinu, I. A.; Meier, W. Molecular organization and dynamics in polymersome membranes: A lateral diffusion study. *Macromolecules* **2014,** *47* (21), 7588-7596.
65. Tabaei, S. R.; Choi, J.-H.; Haw Zan, G.; Zhdanov, V. P.; Cho, N.-J. Solvent-assisted lipid bilayer formation on silicon dioxide and gold. *Langmuir* **2014,** *30* (34), 10363-10373.

66. Valeur, E.; Bradley, M. Amide bond formation: beyond the myth of coupling reagents. *Chemical Society Reviews* **2009,** *38* (2), 606-631.
67. Huang, C.-J.; Cho, N.-J.; Hsu, C.-J.; Tseng, P.-Y.; Frank, C. W.; Chang, Y.-C. Type I collagen-functionalized supported lipid bilayer as a cell culture platform. *Biomacromolecules* **2010,** *11* (5), 1231-1240.
68. Kranz, R. G.; Richard-Fogal, C.; Taylor, J.-S.; Frawley, E. R. Cytochrome c biogenesis: mechanisms for covalent modifications and trafficking of heme and for heme-iron redox control. *Microbiol. Mol. Biol. Rev.* **2009,** *73* (3), 510-528.
69. Zhu, H.; Mumtaz, F.; Zhang, C.; Tan, L.; Liu, S.; Zhang, Y.; Pan, C.; Wang, Y. A rapid approach to prepare poly (2-methyl-2-oxazoline)-based antifouling coating by UV irradiation. *Applied Surface Science* **2017,** *426*, 817-826.
70. Yorulmaz Avsar, S.; Jackman, J. A.; Kim, M. C.; Yoon, B. K.; Hunziker, W.; Cho, N.-J. Immobilization strategies for functional complement convertase assembly at lipid membrane interfaces. *Langmuir* **2017,** *33* (29), 7332-7342.
71. Muenzner, J.; Pletneva, E. V. Structural transformations of cytochrome c upon interaction with cardiolipin. *Chemistry and physics of lipids* **2014,** *179*, 57-63.
72. Alakoskela, J.-M.; Jutila, A.; Simonsen, A. C.; Pirneskoski, J.; Pyhäjoki, S.; Turunen, R.; Marttila, S.; Mouritsen, O. G.; Goormaghtigh, E.; Kinnunen, P. K. Characteristics of fibers formed by cytochrome c and induced by anionic phospholipids. *Biochemistry* **2006,** *45* (45), 13447-13453.
73. Pinheiro, T. J.; Watts, A. Resolution of individual lipids in mixed phospholipid membranes and specific lipid-cytochrome c interactions by magic-angle spinning solid-state phosphorus-31 NMR. *Biochemistry* **1994,** *33* (9), 2459-2467.
74. Pinheiro, T. J.; Watts, A. Lipid specificity in the interaction of cytochrome c with anionic phospholipid bilayers revealed by solid-state 31P NMR. *Biochemistry* **1994,** *33* (9), 2451-2458.
75. Brown, D.; London, E. Functions of lipid rafts in biological membranes. *Annual review of cell and developmental biology* **1998,** *14* (1), 111-136.
76. Zhao, Y.; Xu, J.-X. The operation of the alternative electron-leak pathways mediated by cytochrome c in mitochondria. *Biochemical and biophysical research communications* **2004,** *317* (4), 980-987.
77. Traylor, T. G.; Kim, C.; Richards, J. L.; Xu, F.; Perrin, C. L. Reactions of iron (III) porphyrins with oxidants. Structure-reactivity studies. *Journal of the American Chemical Society* **1995,** *117* (12), 3468-3474.
78. Tanner, P.; Balasubramanian, V.; Palivan, C. G. Aiding nature's organelles: artificial peroxisomes play their role. *Nano letters* **2013,** *13* (6), 2875-2883.
79. Belluati, A.; Craciun, I.; Liu, J.; Palivan, C. G. Nanoscale enzymatic compartments in tandem support cascade reactions in vitro. *Biomacromolecules* **2018,** *19* (10), 4023-4033.
80. Belikova, N. A.; Vladimirov, Y. A.; Osipov, A. N.; Kapralov, A. A.; Tyurin, V. A.; Potapovich, M. V.; Basova, L. V.; Peterson, J.; Kurnikov, I. V.; Kagan, V. E. Peroxidase activity and structural transitions of cytochrome c bound to cardiolipin-containing membranes. *Biochemistry* **2006,** *45* (15), 4998-5009.
81. Lefrançois, P.; Vajrala, V. S. R.; Arredondo, I. B.; Goudeau, B.; Doneux, T.; Bouffier, L.; Arbault, S. Direct oxidative pathway from amplex red to resorufin revealed by in situ confocal imaging. *Physical Chemistry Chemical Physics* **2016,** *18* (37), 25817-25822.
82. Chertkova, R. V.; Brazhe, N. A.; Bryantseva, T. V.; Nekrasov, A. N.; Dolgikh, D. A.; Yusipovich, A. I.; Sosnovtseva, O.; Maksimov, G. V.; Rubin, A. B.; Kirpichnikov, M. P. New insight into the mechanism of mitochondrial cytochrome c function. *PloS one* **2017,** *12* (5), e0178280.